Non-uniformly and totally polarized beams propagating through chiral media

Gemma Piquero[a,*], J. C. G. de Sande[b], Juan C. Suárez-Bermejo[c], Massimo Santarsiero[d]

[a]*Departamento de Óptica, Universidad Complutense de Madrid, Plaza de las Ciencias s/n, 28040Madrid, Spain*
[b]*ETSIS de Telecomunicación, Universidad Politécnica de Madrid, Campus Sur, 28031 Madrid, Spain*
[c]*Materials Science Department, Universidad Politécnica de Madrid, Avda. de la Memoria, 28040 Madrid, Spain*
[d]*Dipartimento di Ingegneria Industriale, Elettronica e Meccanica, Università Roma Tre, Via V. Volterra 62, 00146 Rome, Italy*

Abstract

Non-uniformly and totally polarized (NUTP) beams propagating through chiral media are investigated. These beams have been proved to be useful in fields like polarimetry for the determination of the Mueller matrix of a sample, particle manipulation, etc. In this work, we consider the effects of a chiral medium (i.e., a medium exhibiting circular birefringence and circular dichroism) on the propagation of such beams, and we study the evolution of the transverse irradiance and polarization patterns, both inside the sample and in the free space after the sample, in connection with the optical properties of the medium. In particular, we focus on a class of NUTP beams that preserve their transverse irradiance and polarization pattern during paraxial propagation, in free space or through ABCD optical systems, and the advantages of using them. Conditions are established such that beams remain polarization-invariant after exiting the chiral medium, and simple procedures are presented to gain information about the optical properties of a chiral sample through a suitable choice of the input beam and irradiance measurements across the section of the output beam. These findings highlight the potential of NUTP beams as a versatile tool for investigating optical activity in several

*Corresponding author
Email address: piquero@ucm.es (Gemma Piquero)

fields, such as Pharmacology, Medicine, and Biology.

Keywords: Polarization, Propagation, Structured Light, Optical activity

1. Introduction

Non-uniformly totally polarized beams are beams whose polarization state changes from one point to another across their transverse section. Early research on NUTP beams explored their generation by interferometric methods [1, 2] or using semiconductor lasers [3]. After the development of spatial light modulators (SLMs), many methods have been described to obtain NUTP beams using this type of system (see, for example, [4–7]). Simple cases of NUTP beams are radially, azimuthally, and spirally polarized beams [8–19]. The introduction of NUTP beams has found applications, among others, in fields such as optical tweezers, particle manipulation, microscopy, and polarimetry, where the presence of different polarization states throughout the beam cross section makes the determination of the Mueller matrix of a sample faster and more accurate (see, for example, [20] and references therein).

The polarization pattern across the transverse section of a NUTP beam generally changes with free propagation. However, this does not happen for some kinds of beam, such as radially, azimuthally, and spirally polarized beams, whose polarization pattern remains invariant upon free-space propagation. Actually, this would be a desirable property for a NUTP in various applications, such as Mueller polarimetry with NUTP beams [21–25], because in such a case it is often necessary to focus the input beam on a specific region of interest and, conversely, to suitably enlarge the output beam to fit the detector size, using optical systems that can alter the polarization pattern of the beam. Therefore, using beams that preserve their polarization profile during propagation would be particularly advantageous, as it ensures that the polarization pattern remains stable and well-defined at any distance from the sample, and the use of additional optical elements could be avoided at all.

Here we focus our attention on the propagation of NUTP beams through chiral media, i.e., media that present optical activity, which mainly manifests itself as circular birefringence (CB) and circular dichroism (CD). CB is defined as the ability of certain substances to rotate the plane of polarization of linearly polarized light as it passes through them. This is due to the fact that the refractive indices of the substance for the right- and left-circularly

polarized light are different. For CB measurements, a simple experimental setup is often used, with only a linear polarizer at the input and another at the output of the sample to detect the rotation angle. The input light is always linearly polarized by the first polarizer, while the second polarizer must be rotated until a maximum (or a minimum) of the transmitted irradiance is observed [26, 27]. Of course, such a system does not provide any information on how the sample behaves for other input polarization states.

CD is the ability of the sample to absorb the left- and right-handed circular components of light differently. Detection of CD is commonly used in biochemistry and biology. For example, it allows the identification of different components of biological samples, the assignment of secondary structures, the characterization of the folding state of proteins, etc. [28–30].

The behavior of some biological systems is directly related to the chirality of some substances [31, 32]. Examples of substances that exhibit CB are nucleic acids and proteins [33]. Measurement of the optical activity of proteins gives us information about their secondary structure [34].

The propagation of different structured beams in chiral media, such as Airy beams, Airy- Gaussian beams, vortex beams, stochastic beams, etc., has been investigated [35–41]. These studies show that chirality allows control of the degree of polarization, coherence, chirp, and topological charge and propagation dynamics, highlighting chirality as a tool for manipulating structured light. In the present work changes in polarization and irradiance due to the propagation through chiral media are analyzed for NUTP beams expressed as combinations of higher-order Gaussian beams. Although a decomposition of this kind is possible for any paraxial beam, it turns out to be particularly useful when the number of involved component beams is small. This is the case, for example, of NUTP that are designed to preserve their transverse polarization pattern during free propagation. Moreover, some practical tools using beams of this kind are also proposed for the characterization of chiral media, enabling easy and quick recovery of their birefringence and dichroism parameters.

The starting point of our analysis is the possibility of describing any paraxial beam as the superposition of Hermite-Gaussian and/or Laguerre-Gaussian modes. In the case of vector fields, two orthogonally polarized components will be expressed, in general, as different combinations of Gaussian modes. These expansions allow explicit expressions to be given for the field propagating inside a chiral medium.

In particular, it will be shown that even fields that would preserve their

transverse polarization pattern during propagation in free space do not retain such a property inside a chiral medium. This is not surprising because the two circularly polarized components of the field propagate with different laws. Less obvious is the fact that such kind of beams do not present any longer a propagation-invariant polarization profile even when they exit the chiral medium and propagate in the free space. We find a condition ensuring that the beam emerging from the sample remains invariant upon free-space propagation, of course, although with a different polarization pattern from that of the input beam. This condition basically consists of the requirement that the impinging beam is suitably *collimated*, in a sense that will be specified, when it enters the sample. As we pointed out earlier, this property is of particular relevance when NUTP beams are used in techniques where the polarization pattern of the beam of the exit beam has to be detected just after the sample.

Further results concern the possibility of recovering the optical parameters of a chiral medium by letting a suitable NUTP beam impinge on it and detecting the irradiance profile of the emerging beam. In fact, it is shown that the presence of CB and CD can be easily detected by visual analysis of the transverse profile of the output beam and that a quantitative evaluation of such parameters can be carried out by measuring the irradiance in three distinct points across any transverse plane of the output beam. For this purpose, a simple optical setup is proposed.

The paper is structured as follows. After this introductory part, Sec. 2 is devoted to the description of the tools used to study the paraxial propagation of the scalar and vector fields, of the parameters aimed at quantifying the chirality properties of materials, and of the techniques used to describe the polarization of light. Paraxial propagation inside chiral media is studied in Sec. 3, while the specific case of collimated beams is treated in Sec. 4. The effects of chiral media on the propagation of collimated NUTP beams are investigated in section 5, while the setup proposed to detect circular dichroism and circular birefringence is presented in Sec. 6. The main results are summarized in section 7.

2. Preliminaries

This section compiles the basic concepts related to light polarization and propagation in chiral media that will be used later in this work.

2.1. Paraxial propagation of scalar fields

Within the paraxial approximation, a possible way to address the propagation of a scalar field consists in expressing the initial one in terms of Gaussian modes, whose propagation can be given in closed form. This approach can be implemented in both rectangular and polar coordinates, where the Hermite–Gaussian (HG) or Laguerre–Gaussian (LG) modes, respectively, can be used [42]. In the former case, the basis functions are

$$\mathrm{HG}_{nm}(\boldsymbol{r}; w_0) = \frac{1}{w_0}\sqrt{\frac{2^{-n-m+1}}{\pi\, n!\, m!}}\; H_n\left(\frac{\sqrt{2}\,x}{w_0}\right) H_m\left(\frac{\sqrt{2}\,y}{w_0}\right) \exp\left(-\frac{x^2+y^2}{w_0^2}\right) \;, \tag{1}$$

where (x, y) are the rectangular coordinates of $\boldsymbol{r}$, H_n is the Hermite polynomial of order n, and w_0 is the spot size, which fixes the transverse extent of the modes at their waist.

Analogously, for polar coordinates (r, ϑ), the Laguerre–Gaussian modes can be expressed as [42]

$$\mathrm{LG}_{ps}(\boldsymbol{r}; w_0) = \frac{1}{w_0}\sqrt{\frac{2\,p!}{\pi\,(p+|s|)!}}\; L_p^{|s|}\left(\frac{2\,r^2}{w_0^2}\right)\left(\frac{\sqrt{2}\,r}{w_0}\right)^{|s|} \mathrm{e}^{-(r/w_0)^2}\mathrm{e}^{-\mathrm{i}s\vartheta} \;, \tag{2}$$

where $L_p^{|s|}$ is the generalized Laguerre polynomial of order p and index s.

We will denote both families of Gaussian modes by $\Psi_h(\boldsymbol{r}; w_0)$, regardless of the specific coordinate system we are using, where a single index (h) is formally used, whose meaning depends on the particular class of functions: it can represent either the indexes (n and m) of the two Hermite polynomials involved in the definition of HG functions or the two parameters (p and s) specifying a generalized Laguerre polynomial for the case of LG modes.

Since Gaussian functions form a complete set in L^2, any paraxial beam can be written as a superposition of modes of the above types, with arbitrary w_0. In particular, across the plane $z = 0$ we have

$$V_0(\boldsymbol{r}) = \sum_h c_h\, \Psi_h(\boldsymbol{r}; w_0) \;, \tag{3}$$

where

$$c_h = \int V_0(\boldsymbol{r})\; \Psi_h^*(\boldsymbol{r}; w_0)\; \mathrm{d}\boldsymbol{r} \;, \tag{4}$$

the integral being extended to the whole plane $z = 0$, where the asterisk denotes complex conjugation. The field propagated at a distance z is therefore evaluated taking into account the effects of propagation on each of the modes. The latter, in fact, keep their initial form, up to a scaling factor, and acquire both a spherical curvature and a phase depending on the mode indices. More precisely, we have

$$V_z(\boldsymbol{r}) = \frac{w_0}{w(z)}\, e^{-\mathrm{i}[kz+\Phi(z)]} \exp\left(-\frac{\mathrm{i}kr^2}{2R(z)}\right) \sum_h\, c_h\, \Psi_h[\boldsymbol{r}; w(z)]\, e^{-\mathrm{i}N(h)\Phi(z)}, \quad (5)$$

with $k = nk_0$ the wave number, where n is the refractive index of the medium, $k_0 = 2\pi/\lambda_0$ and λ_0 the wavelength in vacuum. Furthermore,

$$w(z) = w_0\sqrt{1+\left(\frac{z}{L}\right)^2};\; R(z) = z\left[1+\left(\frac{L}{z}\right)^2\right];\; \Phi(z) = \arctan\left(\frac{z}{L}\right), \quad (6)$$

where $L = kw_0^2/2$ is the Rayleigh distance. The parameter $N(h)$ is related to the modes indexes. It equals $n + m$ for HG modes and $2p + |s|$ for LG modes, and appears in the phase term $[N(h) - 1]\Phi(z)$. The latter term is known as *phase anomaly* or *Gouy phase* [43].

It is important to stress that, since each of the modes is shape-invariant during propagation, the phase anomaly is the only responsible for the fact that a general beam changes its shape during propagation [44, 45]. Therefore, if we limit the sum in Eq. (5) to modes giving rise to one and the same value of N, we obtain a propagated field that, apart from a uniform phase and a spherical curvature, is an exact replica of the original one, scaled by the factor $w(z)/w_0$.

2.2. Paraxial propagation of vector fields

Within the paraxial approximation, a typical electric field $\boldsymbol{E}$, having transverse components E_x and E_y, can be described by means of the Jones vector, defined as

$$\boldsymbol{E} = \begin{pmatrix} E_x \\ E_y \end{pmatrix}. \quad (7)$$

The field components E_x and E_y represent the amplitudes of two linearly polarized fields (along x and y, respectively). However, since we will be interested in beam propagating through a chiral medium, it is also useful to

represent the same field as the superposition of circularly polarized states, namely,

$$\boldsymbol{E} = E_R\,\mathbf{u}_R + E_L\,\mathbf{u}_L\ , \tag{8}$$

with

$$\mathbf{u}_R = \frac{1}{\sqrt{2}}\begin{pmatrix} 1 \\ \mathrm{i} \end{pmatrix}\ ; \quad \mathbf{u}_L = \frac{1}{\sqrt{2}}\begin{pmatrix} 1 \\ -\mathrm{i} \end{pmatrix}\ . \tag{9}$$

It is clear from Eqs. (7)-(9) that

$$\begin{cases} E_x = \dfrac{1}{\sqrt{2}}(E_R + E_L)\,, \\ \\ E_y = \dfrac{\mathrm{i}}{\sqrt{2}}(E_R - E_L)\,, \end{cases} \quad \text{and} \quad \begin{cases} E_R = \dfrac{1}{\sqrt{2}}(E_x - \mathrm{i}E_y)\,, \\ \\ E_L = \dfrac{1}{\sqrt{2}}(E_x + \mathrm{i}E_y)\,. \end{cases} \tag{10}$$

The propagation of a vector field is addressed by letting the two components propagate separately. In particular, for each of the two component fields, an expansion in Gaussian modes can be used of the form of that in Eq. (5). If the field propagates in vacuum or in a homogeneous medium, both components experiment the same refractive index, and the same formula can be used for both. In this case, it is possible to devise a class of fields whose transverse polarization pattern does not change during propagation, except for a transverse scaling factor [45, 46]. To this aim, it is sufficient that all the Gaussian modes appearing in the expansions of the two components be characterized by one and the same value of N. This guarantees, on the one hand, that each component does not change its transverse shape during propagation, as we saw in the previous subsection; on the other hand, that even the phase relation between the two components does not change, thus preserving the polarization of their superposition during propagation. Furthermore, the transverse polarization pattern is preserved also for propagation through any ABCD optical system because within such systems the beam parameters (i.e., spot size, curvature radius, and phase anomaly) of all the component modes propagate with the same law.

Beams with invariant polarization patterns offer interesting possibilities. They are due to the fact that, when a beam of this type passes through a linear deterministic element characterized by Jones or Mueller matrices (such as a polarizer or a phase plate), its polarization pattern changes, but the new pattern remains unchanged during subsequent propagation of the exit beam [45, 46].

More complex is the problem of a beam propagating through an anisotropic medium. In particular, we will be interested in chiral media, which present different dielectric properties for left- and right-handed circular polarization. Of course, in such a case, a field decomposition in terms of circular polarization states is more appropriate. This will be dealt with in Sec. 3.

2.3. Chiral media

A chiral medium, or optically active medium, is a medium that exhibits optical activity (OA). Optical activity can be considered as the combined action of two effects: circular birefrigence (CB) and circular dichroism (CD). Both such effects can be taken into account by a complex refractive index that depends on the handedness of the circular polarization state of the propagating light. We denote by $\tilde{n}_j$ $(j = R, L)$ the complex refractive index for right- and left-handed circularly polarized light.

The real and imaginary parts of $\tilde{n}_j$ $(j = R, L)$, namely n_j and κ_j, are the refractive index and the extinction coefficient for right- and left-handed circularly polarized fields, respectively. Therefore, circular birefringence and circular dichroism can be ascribed to the difference of the complex refractive indices as

$$\Delta\tilde{n} = (n_R - n_L) - i\,(\kappa_R - \kappa_L) = \Delta n - i\,\Delta\kappa. \tag{11}$$

An effect of circular birefringence of a chiral medium consists of its ability to rotate the polarization ellipse of light passing through it. Depending on the sense of rotation, the medium will be said to be dextrorotatory or levorotatory (if the rotation is clockwise or counterclockwise, respectively). For example, linearly polarized light can be thought of as the superposition of right- and left-handed circularly polarized light with equal amplitudes. Since these components travel at different velocities, their mutual phase varies during propagation, and this results in a change in the azimuth of the propagated light.

The rotation angle, say Γ, that the polarization of the input beam undergoes when traveling a distance d within the medium turns out to be

$$\Gamma = \frac{k_0\,\Delta n\,d}{2}, \tag{12}$$

where d is the length of the sample. It can be measured directly by means of two linear polarizers, placed at the input and output, respectively, of the sample [47].

Analogously, if the medium presents circular dichroism, the following parameter can be defined:

$$\Gamma' = \frac{k_0 \, \Delta\kappa \; d}{2}. \tag{13}$$

In such a case, the ratio between the amplitudes of the two circularly polarized components changes during propagation, so that the effect is no longer a pure rotation but a change in the shape of the polarization ellipse is expected.

2.4. Stokes-Mueller formalism

Within the Stokes-Mueller formalism, the polarization of a paraxial field is represented by its Stokes vector, whose elements (the Stokes parameters) can be defined in terms of the field components E_x and E_y of the Jones vector in Eq. (7) as [48]

$$\mathbf{S} = \begin{pmatrix} S_0 \\ S_1 \\ S_2 \\ S_3 \end{pmatrix} = \begin{pmatrix} |E_x|^2 + |E_y|^2 \\ |E_x|^2 - |E_y|^2 \\ 2\,\mathrm{Re}\{E_x^* E_y\} \\ 2\,\mathrm{Im}\{E_x^* E_y\} \end{pmatrix} . \tag{14}$$

Therefore, S_0 represents the total irradiance, while S_1 gives the difference between the polarized light components at $0°$ and $90°$, and the same holds for S_2 for polarizations at $+45°$ and $-45°$, and for S_3 for circularly dextro- and levo-polarized light. The four Stokes parameters can be obtained experimentally from irradiance measures, using a polarizer at different angles and a quarter-wave phase plate placed before the polarizer [48].

It is also useful to introduce the *normalized* Stokes vector $\mathbf{s}$, having components $s_i = S_i/S_0$, $(i = 1, 2, 3)$, so that

$$\mathbf{S} = S_0 \begin{pmatrix} 1 \\ s_1 \\ s_2 \\ s_3 \end{pmatrix} . \tag{15}$$

In terms of the normalized Stokes parameters, the degree of polarization of the field can be calculated as

$$P = \sqrt{s_1^2 + s_2^2 + s_3^2} \, . \tag{16}$$

The action of an optical system on an incident beam is described by the 4×4 Mueller matrix of the system, that is,

$$\widehat{M} = \begin{pmatrix} m_{00} & m_{01} & m_{02} & m_{03} \\ m_{10} & m_{11} & m_{12} & m_{13} \\ m_{20} & m_{21} & m_{22} & m_{23} \\ m_{30} & m_{31} & m_{32} & m_{33} \end{pmatrix}, \tag{17}$$

in such a way that the relationship between the Stokes vectors at the output ($\mathbf{S}^{out}$) and at the input ($\mathbf{S}^{in}$) of the sample is given by

$$\mathbf{S}^{out} = \widehat{M}\, \mathbf{S}^{in} \, . \tag{18}$$

Note that, in general, all previous parameters depend on $\mathbf{r}$, so that the state of polarization may be different across the beam transverse section.

3. Paraxial propagation through chiral media

To study the propagation of a vector field through a chiral medium, we start from the expansion of a typical field across the starting plane in circularly polarized components, as given in Eq. (8), i.e.,

$$\boldsymbol{E}_0(\boldsymbol{r}) = \begin{pmatrix} E_{0x}(\boldsymbol{r}) \\ E_{0y}(\boldsymbol{r}) \end{pmatrix} = E_{0R}(\boldsymbol{r})\, \mathbf{u}_R + E_{0L}(\boldsymbol{r})\, \mathbf{u}_L \, , \tag{19}$$

with

$$\begin{cases} E_{0R}(\boldsymbol{r}) = \dfrac{1}{\sqrt{2}} \left[E_{0x}(\boldsymbol{r}) - \mathrm{i} E_{0y}(\boldsymbol{r}) \right] \, , \\ \\ E_{0L}(\boldsymbol{r}) = \dfrac{1}{\sqrt{2}} \left[E_{0x}(\boldsymbol{r}) + \mathrm{i} E_{0y}(\boldsymbol{r}) \right] \, . \end{cases} \tag{20}$$

The two circularly polarized components propagate with different refractive indices and, at a distance z from the starting plane, they can be written as

$$\begin{cases} E_{zR}(\boldsymbol{r}) = \dfrac{1}{\sqrt{2}} \left[E_{zx}^{(R)}(\boldsymbol{r}) - \mathrm{i} E_{zy}^{(R)}(\boldsymbol{r}) \right] \, , \\ \\ E_{zL}(\boldsymbol{r}) = \dfrac{1}{\sqrt{2}} \left[E_{zx}^{(L)}(\boldsymbol{r}) + \mathrm{i} E_{zy}^{(L)}(\boldsymbol{r}) \right] \, , \end{cases} \tag{21}$$

where the superscript (R or L) denotes that the propagation formulas must be used with the corresponding complex refractive index ($\tilde{n}_R$ or $\tilde{n}_L$). In particular, the two components will propagate with different refractive indices (n_L and n_R) and attenuate with different extinction coefficients (κ_L and κ_R).

Finally, we can go back to the Jones vector of the propagated field using again Eq. (10). This gives, explicitly,

$$\boldsymbol{E}_z(\boldsymbol{r}) = \frac{1}{2} \begin{pmatrix} E_{zx}^{(R)}(\boldsymbol{r}) - \mathrm{i}E_{zy}^{(R)}(\boldsymbol{r}) + E_{zx}^{(L)}(\boldsymbol{r}) + \mathrm{i}E_{zy}^{(L)}(\boldsymbol{r}) \\ \\ \mathrm{i}E_{zx}^{(R)}(\boldsymbol{r}) + E_{zy}^{(R)}(\boldsymbol{r}) - \mathrm{i}E_{zx}^{(L)}(\boldsymbol{r}) + E_{zy}^{(L)}(\boldsymbol{r}) \end{pmatrix} . \tag{22}$$

The propagation of the field can be studied through the expansion in Gaussian beams presented in the previous Section. Therefore, Eqs. (5) and (6) can be used, where k must be replaced by $k_R = n_R k_0$ or $k_L = n_L k_0$, depending on the handedness of the circular polarization of the component field. Then, the two components will be characterized by two different Rayleigh distances and then by two different beam widths, two different curvature radii, and two different Gouy phases. Furthermore, the two components will be attenuated by two different factors, i.e., $e^{-k_0 \kappa_R z}$ or $e^{-k_0 \kappa_L z}$.

This implies, in particular, that the condition we recalled in the previous Section about the propagation invariance of the transverse polarization pattern (i.e., the same value of N for all the contributing modes) does not hold any longer. More precisely, it holds for each of the components (R and L), but it does not guarantee that the two components spread at the same rate and maintain the same amplitude and phase in any transverse plane. Therefore, in general, both the irradiance and the polarization pattern of the field change upon propagation through the chiral medium.

As an example of beams that preserve their transverse polarization pattern during free propagation, we consider a radially polarized donut beam having an electric field given by

$$\boldsymbol{E}_0(\boldsymbol{r}) = E_0 \, e^{-(r/w_0)^2} \begin{pmatrix} x \\ y \end{pmatrix} . \tag{23}$$

where E_0 is an amplitude factor and w_0 is the spot size.

It can be easily recognized as the superposition of a HG_{10} mode polarized along x and a HG_{01} mode polarized along y. In fact, from Eq. (1) we have

$$\boldsymbol{E}_0(\boldsymbol{r}) = A_0 \begin{pmatrix} \mathrm{HG}_{10}(\boldsymbol{r}; w_0) \\ \mathrm{HG}_{01}(\boldsymbol{r}; w_0) \end{pmatrix} , \tag{24}$$

with

$$A_0 = E_0 \, \frac{w_0^2}{2} \sqrt{\frac{\pi}{2}} \, . \tag{25}$$

Its circular-polarization components are, according to Eqs. (20) and (2),

$$\begin{cases} E_{0R}(\boldsymbol{r}) = \dfrac{E_0}{\sqrt{2}} \, (x - iy) \; e^{-(r/w_0)^2} = A_0 \; \mathrm{LG}_{01}(\boldsymbol{r}; w_0) \, , \\ \\ E_{0L}(\boldsymbol{r}) = \dfrac{E_0}{\sqrt{2}} \, (x + iy) \; e^{-(r/w_0)^2} = A_0 \; \mathrm{LG}_{0-1}(\boldsymbol{r}; w_0) \; , \end{cases} \tag{26}$$

whose propagation through the chiral medium can be evaluated by means of Eq. (5), where LG beams are chosen as the modes and, for each component, only one term appears in the sum, i.e., $h = (p, s) = (0, 1)$ and $h = (0, -1)$, respectively. Furthermore, for each polarization the corresponding refractive index has to be considered. Explicitly, this leads to

$$\begin{cases} E_{zR}(\boldsymbol{r}) = \dfrac{A_0 w_0}{w_R(z)} \; e^{-\mathrm{i}[n_R k_0 z + 2\Phi_R(z)]} \; e^{-\kappa_R k_0 z} \, e^{-\frac{\mathrm{i}kr^2}{2R_R(z)}} \, \mathrm{LG}_{01}[\boldsymbol{r}; w_R(z)] \, , \\ \\ E_{zL}(\boldsymbol{r}) = \dfrac{A_0 w_0}{w_L(z)} \; e^{-\mathrm{i}[n_L k_0 z + 2\Phi_L(z)]} \; e^{-\kappa_L k_0 z} \, e^{-\frac{\mathrm{i}kr^2}{2R_L(z)}} \, \mathrm{LG}_{0-1}[\boldsymbol{r}; w_L(z)] \; , \end{cases} \tag{27}$$

where $w_j(z)$, $R_j(z)$, and $\Phi_j(z)$ (with $j = R, L$) are given by Eq. (6), with $L = L_j = n_j \pi w_0^2 / \lambda_0$.

In Fig. 1 irradiance and polarization patterns are shown, obtained after propagation of the field given in Eq. (23) within a chiral medium, at different distances d from the input plane. The parameters used are $\lambda_0 = 632.8$ nm, $w_0 = 0.01$ mm, $n_L = 1.5$ and $n_R = 2.0$, without circular dichroism ($\kappa_R = \kappa_L = 0$). As can be seen, during propagation, the beam polarization changes from linear to elliptical at any fixed point of the transverse beam section. This can be understood by taking into account that the ellipticity of the polarization ellipse (expressed through the angle χ) is related to the parameter s_3 ($= \sin 2\chi$) [26], which gives the difference between the intensities of right-handed and left-handed circularly polarized components. Since the chiral medium affects the two components differently (see Eq. (27)), it is clear that, in general, the amplitudes of these two components change in a different way at any point $(\boldsymbol{r}, z > 0)$, and the polarization state from linear may become elliptical, independently of their phase difference, which is related to the azimuth.

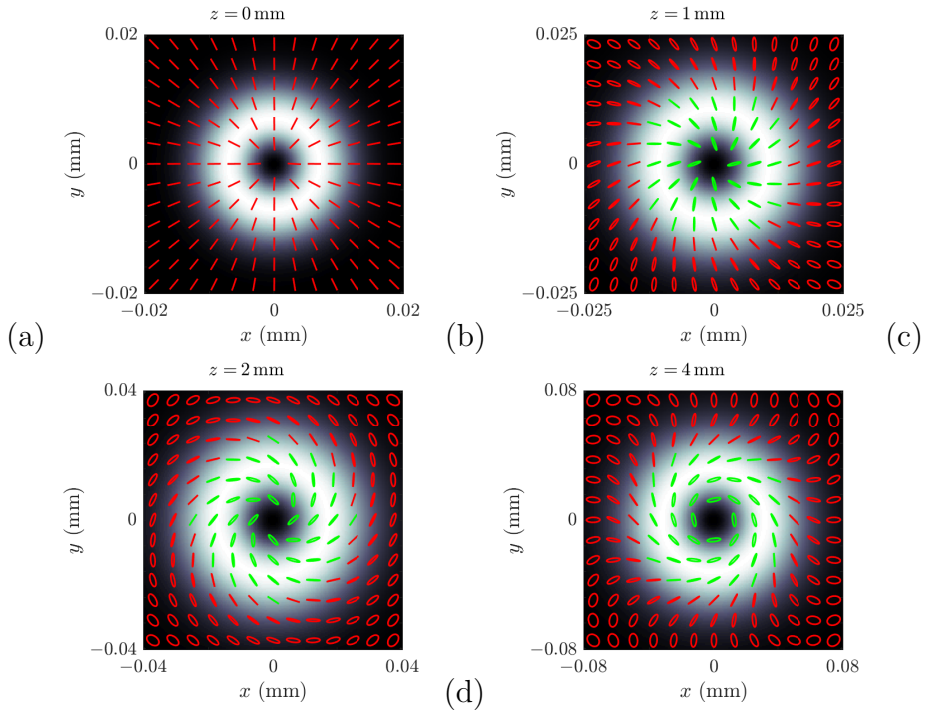

Figure 1: Irradiance and polarization pattern inside a sample with $n_L = 1.5$, $n_R = 2$, $\kappa_L = \kappa_R = 0$, $\lambda_0 = 632.8$ nm and $w_0 = 0.01$ mm, calculated for the beam given by Eq. (23). The propagation distance inside the chiral medium is (a) $z = 0$ mm; (b) $d = 1$ mm; (c) $d = 2$ mm; and (d) $d = 4$ mm. Note that the representation area has been adjusted to the growing beam size. Green (red) ellipses represent right-handed (left-handed) polarization.

Basically, the same conclusions hold, in general, for the beam that emerges from the chiral sample and propagates in the free space. In fact, although the modes are exactly the same as those of the input one and now all of them experiment the same refractive index, the modes composing the two orthogonal polarizations emerge with different spot sizes and curvature radii so that even in the free space, they propagate with different laws. Therefore, the resulting beam does not present an invariant profile during propagation. In fact, since the spot size grows faster for a beam with a smaller waist size, a distance after the chiral medium will exist where the two orthogonally polarized components have the same spot size, so that the beam is linearly polarized there. For shorter distances (or even longer), the polarization is expected to be generally elliptical.

Such an effect is shown in Fig. 2, where the irradiance and polarization patterns are shown at two distances z from the output plane of the sample. The thickness of the sample has been chosen as $d = 4$ mm, while the other parameters are the same as those of Fig. 1.

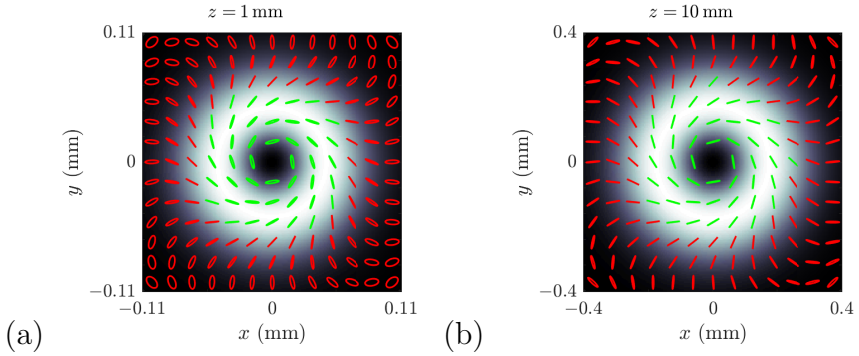

Figure 2: Irradiance and polarization pattern outside a sample with $n_L = 1.5$, $n_R = 2$, $\kappa_L = \kappa_R = 0$, $\lambda_0 = 632.8$ nm and thickness $d = 4$ mm , calculated for the beam given by Eq. (23) with $w_0 = 0.01$ mm. The propagation distance after the output plane of the chiral medium is (a) $z = 1$ mm and (b) $z = 10$ mm. Note that the representation area has been adjusted to the growing beam size. Green (red) ellipses represent right-handed (left-handed) polarization.

4. Collimated beams through chiral media

We mean that a Gaussian mode incident onto the sample is collimated when its Rayleigh distance is much larger than the thickness of the sample and the latter is placed near its waist plane. A beam obtained as a combination of collimated Gaussian modes will be collimated as well. In such a case, since the spot size and curvature radius of the modes do not change significantly when they pass through the sample, the only effect of propagation through the chiral medium is a change in the mutual phase and in the amplitude ratio between the right- and left-polarized components. Therefore, while at the exit face of the sample the polarization pattern of the beam is generally different from that of the input one, it remains unchanged during the subsequent propagation in free space. In other terms, the effect shown at the end of the previous section tends to be negligible, and the beam propagating after the sample presents a propagation-invariant polarization pattern. Such an invariance is also guaranteed for beams propagating through ABCD optical systems.

Furthermore, when the above conditions are satisfied, the propagation through the chiral medium can be dealt with in a much simpler way. In fact, in this case the effect of the sample can be taken into account by a suitable 2×2 Jones matrix [49–52]. Denoting by $\boldsymbol{E}_{in}$ and $\boldsymbol{E}_{out}$ the fields entering and emerging from the sample, respectively, we have

$$\boldsymbol{E}_{out} = \widehat{J}\,\boldsymbol{E}_{in}, \tag{28}$$

where the explicit form of the Jones matrix $\widehat{J}$, derived in the Appendix, is

$$\begin{aligned}\widehat{J} \;&=\; e^{-i\frac{k_0 d}{2}(n_D+n_L)}e^{-\frac{k_0 d}{2}(\kappa_D+\kappa_L)} \\ &\quad\times\begin{pmatrix} \cos(\Gamma - i\Gamma') & -\sin(\Gamma - i\Gamma') \\ \sin(\Gamma - i\Gamma') & \cos(\Gamma - i\Gamma') \end{pmatrix},\end{aligned} \tag{29}$$

with the quantities Γ and Γ' defined in Eqs. (12) and (13).

The effect of the matrix $\widehat{J}$ on an incident field can be better understood if we express it as a product of two commuting matrices in the following way:

$$\begin{aligned}\widehat{J} \;&=\; e^{-i\frac{k_0 d}{2}(n_D+n_L)}e^{-\frac{k_0 d}{2}(\kappa_D+\kappa_L)} \\ &\quad\times\begin{pmatrix} \cosh\Gamma' & i\sinh\Gamma' \\ -i\sinh\Gamma' & \cosh\Gamma' \end{pmatrix}\begin{pmatrix} \cos\Gamma & -\sin\Gamma \\ \sin\Gamma & \cos\Gamma \end{pmatrix}.\end{aligned} \tag{30}$$

The first one is associated with dichroism and is written in terms of hyperbolic functions, while the other one, expressed in terms of trigonometric functions, is associated with birefringence. The latter is identified as a rotation matrix, which demonstrates the rotation of the polarization plane by an angle Γ as the beam passes through the optically active medium.

In view of an experimental characterization of a chiral sample, the Stokes-Mueller formalism is also useful (see Sect. 2.4). The Mueller matrix for a chiral medium turns out to be (see Appendix or references [49, 53]).

$$\widehat{M}_{AO} = e^{-k_0 d(\kappa_R+\kappa_L)}\begin{pmatrix} \cosh 2\Gamma' & 0 & 0 & -\sinh 2\Gamma' \\ 0 & \cos 2\Gamma & -\sin 2\Gamma & 0 \\ 0 & \sin 2\Gamma & \cos 2\Gamma & 0 \\ -\sinh 2\Gamma' & 0 & 0 & \cosh 2\Gamma' \end{pmatrix}. \tag{31}$$

Using Eqs. (15), (18), and (31), the Stokes vector at the output of the chiral sample turns out to be

$$\mathbf{S}^{out} = S_0^{in}\, e^{-k_0 d(\kappa_R+\kappa_L)}\begin{pmatrix} \cosh(2\,\Gamma') - s_3^{in}\sinh(2\,\Gamma') \\ s_1^{in}\cos(2\,\Gamma) - s_2^{in}\sin(2\,\Gamma) \\ s_1^{in}\sin(2\,\Gamma) + s_2^{in}\cos(2\,\Gamma) \\ -\sinh(2\,\Gamma') + s_3^{in}\cosh(2\,\Gamma') \end{pmatrix}. \tag{32}$$

Equation (32), in particular, gives account of the most typical effects encountered when dealing with changes in polarization due to propagation in chiral media. For example, if we consider a linearly polarized input beam with polarization axis at the angle φ with respect to x, we have $\mathbf{s}^{in} = (\cos(2\varphi), \sin(2\varphi), 0)^T$, so that

$$\mathbf{S}^{out} = S_0^{in}\, e^{-k_0 d(\kappa_R+\kappa_L)}\, \cosh(2\,\Gamma') \begin{pmatrix} 1 \\ \operatorname{sech}(2\,\Gamma')\, \cos\left[(2(\varphi+\Gamma)\right] \\ \operatorname{sech}(2\,\Gamma')\, \sin\left[(2(\varphi+\Gamma)\right] \\ -\tanh(2\,\Gamma') \end{pmatrix} . \tag{33}$$

If $\Gamma' \neq 0$ (i.e., $\Delta\kappa \neq 0$), the polarization of the output beam becomes generally elliptical, but if $\Gamma' = 0$ (i.e., $\Delta\kappa = 0$) the medium only produces a rotation of the polarization direction by angle Γ.

Conversely, a circularly polarized input beam, i.e., $\mathbf{s}^{in} = (0, 0, \pm 1)^T$, does not change its polarization state because

$$\mathbf{S}^{out} = S_0^{in}\, e^{-k_0 d(\kappa_R+\kappa_L)}\, \left[\cosh(2\,\Gamma') \mp \sinh(2\,\Gamma')\right] \begin{pmatrix} 1 \\ 0 \\ 0 \\ \pm 1 \end{pmatrix} . \tag{34}$$

We could also verify that, in general, if the input light is uniformly totally polarized, then the degree of polarization remains unchanged and equal to 1, as expected. Furthermore, for a completely unpolarized input beam, i.e., when $\mathbf{s}^{in} = (0, 0, 0)^T$, the output beam is partially polarized, because

$$\mathbf{S}^{out} = S_0^{in}\, e^{-k_0 d(\kappa_R+\kappa_L)}\, \cosh(2\,\Gamma') \begin{pmatrix} 1 \\ 0 \\ 0 \\ -\tanh\left(2\Gamma'\right) \end{pmatrix} . \tag{35}$$

In this case, the degree of polarization depends on the CD as

$$P = \tanh(2\,\Gamma'), \tag{36}$$

and the polarized part of the beam is circularly polarized. This is due to the fact that a completely unpolarized field can be thought of as the superposition of two mutually uncorrelated fields with equal powers and orthogonal circular polarizations. In the presence of CD, during propagation the amplitudes of the two fields decrease with different rates, and one of the two polarizations tends to overrule the other.

5. Effects of a chiral medium on collimated NUTP beams

Interesting effects can be observed when the beam passing through the chiral medium presents a nonuniform transverse polarization pattern. In this case we can use the expressions derived in the previous section, but with the Stokes parameters depending on the coordinate $\mathbf{r}$ across the transverse plane. In particular, those results suggest that modifications in the irradiance distribution of the input beams can be used to get information about the optical parameters of the medium.

For example, the total irradiance, which corresponds to the first Stokes parameter, is obtained from Eq. (32) as

$$S_0^{out}(\boldsymbol{r}) = C S_0^{in}(\boldsymbol{r}) \left[\cosh(2\,\Gamma') - s_3^{in}(\boldsymbol{r})\, \sinh(2\,\Gamma')\,\right], \tag{37}$$

with constant $C = \exp\left[-k_0 d(\kappa_R + \kappa_L)\right]$. It is seen that the transverse irradiance profile of the output beam is affected by the value of the third normalized Stokes parameter of the input beam and by the circular dichroism Γ' (but not on the circular birefringence Γ) of the sample. Therefore, the transverse irradiance profile of the input beam turns out to be modulated by the function

$$\rho(\boldsymbol{r}) = \frac{S_0^{out}(\boldsymbol{r})}{S_0^{in}(\boldsymbol{r})} = C \left[\cosh(2\,\Gamma') - s_3^{in}(\boldsymbol{r})\, \sinh(2\,\Gamma')\right], \tag{38}$$

and the determination of Γ' could be performed by exploiting the variations of s_3^{in} across the beam profile.

If the input beam is chosen properly, a simple visual analysis of the transverse irradiance pattern can give useful information about the circular dichroism of the sample. Furthermore, using a beam whose transverse profile does not change during propagation is also useful because in such a case the irradiance pattern can be detected across any transverse plane after the sample, or even after an ABCD optical system, and not necessarily at the output face of the sample. The approach will be illustrated in the following example.

In order to observe spatial variations of the factor ρ, an input beam with spatially varying s_3^{in} must be chosen. To this aim the field of Eq. (23), although with nonuniform and propagation-invariant polarization pattern, cannot be used because it is linearly polarized at any point and $s_3^{in}(\boldsymbol{r}) = 0$ for any $\boldsymbol{r}$. Nonetheless, it is sufficient to multiply its y component by $e^{i\pi/2}$ to obtain

$$\boldsymbol{E}_0(\boldsymbol{r}) = E_0\, e^{-(r/w_0)^2} \begin{pmatrix} x \\ i\,y \end{pmatrix}, \tag{39}$$

for which, from Eq. (14),

$$\begin{cases} S_0^{in}(\boldsymbol{r}) = |E_0|^2\, r^2\, e^{-2(r/w_0)^2} \\ S_1^{in}(\boldsymbol{r}) = |E_0|^2\, r^2\, e^{-2(r/w_0)^2}\, \cos(2\vartheta) \\ S_2^{in}(\boldsymbol{r}) = 0 \\ S_3^{in}(\boldsymbol{r}) = |E_0|^2\, r^2\, e^{-2(r/w_0)^2}\, \sin(2\vartheta)\ , \end{cases} \tag{40}$$

so that

$$s_1^{in}(\boldsymbol{r}) = \cos(2\vartheta)\ , \quad s_2^{in}(\boldsymbol{r}) = 0\ , \quad s_3^{in}(\boldsymbol{r}) = \sin(2\vartheta)\ . \tag{41}$$

The beam polarization pattern continues to be non-uniform and propagation invariant, but its s_3 normalized Stokes parameter takes values ranging from -1 to 1 across the transverse plane. Furthermore, the irradiance profile of the input beam is circularly symmetric because S_0^{in} is independent of ϑ.

From Eq. (37), the corresponding irradiance at the output of a chiral sample turns out to be

$$S_0^{out}(\boldsymbol{r}) = C|E_0|^2\, r^2\, e^{-2(r/w_0)^2}\, [\cosh(2\,\Gamma') - \sin(2\vartheta)\, \sinh(2\,\Gamma')\,]\,, \tag{42}$$

and is shown in Fig. 3 for different values of Γ'. For example, for a 20 mm thick sample and wavelength $\lambda_0 = 632.8$ nm, the selected values of Γ' correspond to $\Delta\kappa = 0$, $\Delta\kappa \simeq 2.5 \cdot 10^{-5}$, $\Delta\kappa \simeq 5 \cdot 10^{-5}$, and $\Delta\kappa \simeq -5 \cdot 10^{-5}$.

A simple visual analysis of the pattern highlights the presence of circular dichroism and gives a qualitative esteem of its entity. A more quantitative analysis can be performed by measuring the irradiance at two points located along a circle, centered on the origin of the axes and with an arbitrary radius, at the angles $\vartheta = \pi/4$ and $\vartheta = -\pi/4$, respectively, corresponding to the angular positions with the minimum or the maximum irradiance. In fact,

$$\frac{S_0^{out}(r, -\pi/4) - S_0^{out}(r, \pi/4)}{S_0^{out}(r, -\pi/4) + S_0^{out}(r, \pi/4)} = \tanh(2\Gamma')\ , \tag{43}$$

which directly allows for the evaluation of Γ'. Note that $|\tanh(t)|$ saturates to 1 when $|t|$ exceeds 2 (approximately). This means that to detect significant changes in irradiance, the thickness d of the chiral medium should be of the

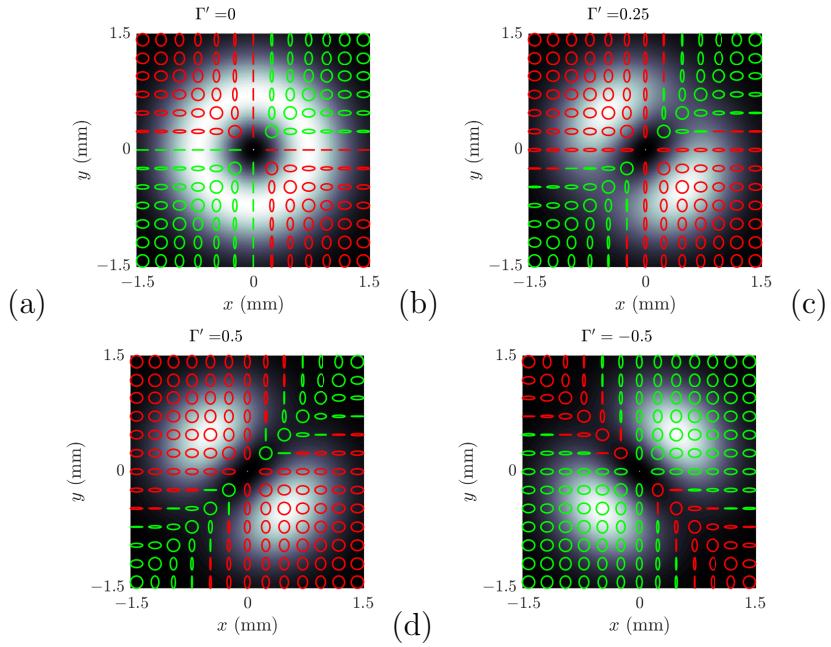

Figure 3: Irradiance at the output of the media with natural optical activity for different absorptions for the example of Eq. (39). (a) $\Gamma' = 0$; (b) $\Gamma' = 0.25$; (c) $\Gamma' = 0.5$; (d) $\Gamma' = -0.5$. Other parameters: $\lambda_0 = 632.8$ nm, $w_0 = 1$ mm. Green (red) ellipses represent right-handed (left-handed) polarization.

same order of magnitude as the ratio between the wavelength used and $\Delta\kappa$ (see Eq. (13)).

Analogous procedures can be devised to detect circular birefringence. In the previous example, the output intensity did not depend on Γ, so the scheme already presented must be suitably modified. A possible solution consists of inserting a linear polarizer after the sample, with its transmission axis along x. The Mueller matrix for such an element is [47]

$$\widehat{M}_x = \frac{1}{2}\begin{pmatrix} 1 & 1 & 0 & 0 \\ 1 & 1 & 0 & 0 \\ 0 & 0 & 0 & 0 \\ 0 & 0 & 0 & 0 \end{pmatrix}, \tag{44}$$

so that the cascade of an active medium and the linear polarizer described

above is represented by a Mueller matrix of the form

$$\widehat{M}_{AOL} = \widehat{M}_x\,\widehat{M}_{AO} = \begin{pmatrix} \cosh(2\Gamma') & \cos(2\Gamma) & -\sin(2\Gamma) & -\sinh(2\Gamma') \\ \cosh(2\Gamma') & \cos(2\Gamma) & -\sin(2\Gamma) & -\sinh(2\Gamma') \\ 0 & 0 & 0 & 0 \\ 0 & 0 & 0 & 0 \end{pmatrix}, \quad (45)$$

which, for a typical input Stokes vector, gives rise to following irradiance after the polarizer:

$$\begin{aligned} S_0^{out}(\boldsymbol{r}) = C\, S_0^{in}(\boldsymbol{r})\, [\cosh(2\,\Gamma') + \cos(2\Gamma)\, s_1^{in}(\boldsymbol{r}) \\ - \sin(2\Gamma)\, s_2^{in}(\boldsymbol{r}) - \sinh(2\Gamma')\, s_3^{in}(\boldsymbol{r})] \,, \end{aligned} \quad (46)$$

with, again, $C = \exp\left[-k_0 d(\kappa_D + \kappa_L)\right]$.

The field in Eq. (39) is not a good choice in this case because, to recover the birefringence term Γ, the coefficients multiplying $\cos(2\Gamma)$ and $\sin(2\Gamma)$ must both be different from zero. A simple way to bring out Γ is to use a radially polarized input beam, of the form given in Eq. (23), for which the irradiance profile is the same as that of the previous example (S_0^{in} of Eq. (40)), but

$$s_1^{in}(\boldsymbol{r}) = \cos(2\vartheta) \,, \quad s_2^{in}(\boldsymbol{r}) = \sin(2\vartheta) \,, \quad s_3^{in}(\boldsymbol{r}) = 0 \,. \quad (47)$$

Such a field gives rise to the following irradiance:

$$S_0^{out}(\boldsymbol{r}) = C\, S_0^{in}(\boldsymbol{r})\, [\cosh(2\,\Gamma') + \cos(2\Gamma + 2\theta)] \,, \quad (48)$$

which is shown in Fig. 4 for $\Gamma' = 0$ (that is $\Delta\kappa = 0$) and different values of Γ. The spot size is $w_0 = 1$ mm and the wavelength is $\lambda = 632.8$ nm. Note that the values of $\Gamma = \pi/4$, $\pi/2$, and $3\pi/4$ correspond to those of a quartz crystal with thicknesses of 2.26 mm, 4.52 mm and 6.78 mm, respectively.

In this case, too, a simple visual analysis of the profile gives information about the presence of optical activity of the sample, which is responsible for a rotation of the intensity profile by an amount of $-\Gamma$. The same pattern is obtained when Γ is increased by an integer multiple of π, corresponding to the fact that phase differences between the two circularly polarized components that are multiple of 2π produce the same effect.

Different values of $\Delta\kappa$ do not modify the angular dependence of the profile, but reduce the contrast of the image, as shown in Fig. 5, plotted for

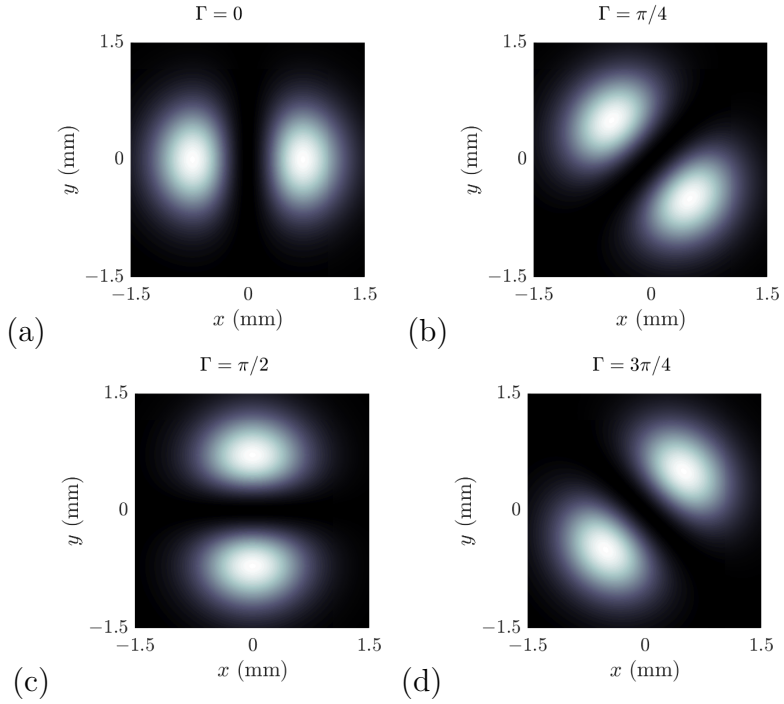

Figure 4: Irradiance at the output of the media with natural optical activity for the example of Eq. (23), with different values of Γ: (a) $\Gamma = 0$; (b) $\Gamma = \pi/4$; (c) $\Gamma = \pi/2$; (d) $\Gamma = 3\pi/4$. ($w_0 = 1$ mm, $\Delta\kappa = 0$).

$\Delta n = 0$. The selected values of Γ' (that is, 0.25, 0.5, 0.75, and 1) correspond to values of $\Delta\kappa \simeq 0.25 \times 10^{-5}$, $\Delta\kappa \simeq 0.5 \times 10^{-5}$, $\Delta\kappa \simeq 0.75 \times 10^{-5}$, and $\Delta\kappa \simeq 1 \times 10^{-5}$, respectively, for a 20 mm thick sample at wavelength $\lambda = 632.8$ nm. Therefore, the same pattern also gives information about the presence of circular dichroism. When $|\Gamma'| \gg 1$ the profile becomes almost annular. Moreover, since only $\cosh(2\Gamma')$ appears in Eq. (37), the sign of Γ' cannot be deduced.

6. An optical scheme for chiral media characterization

The two optical schemes presented in the previous section can be implemented in a unique setup, sketched in Fig. 6. A laser beam is expanded and collimated by means of a microscope objective (MO) and a lens (L). Then, a polarization converter (PC) is used to produce radial polarization. PC may consist, for example, of a vortex half-wave retarder plate [54], an azimuthal

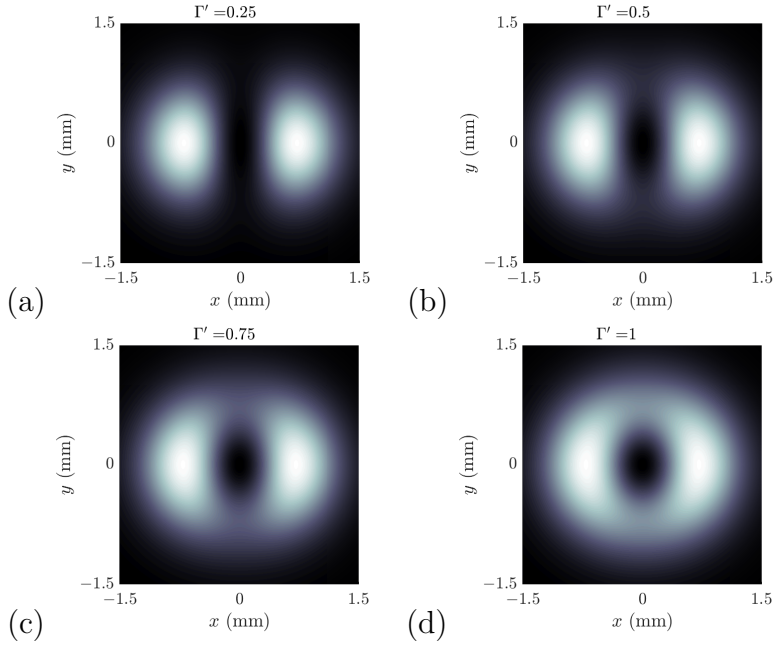

Figure 5: The same as in Fig 4, but for $\Gamma = 0$ and different values of Γ': (a) $\Gamma' = 0.25$; (b) $\Gamma' = 0.5$; (c) $\Gamma' = 0.75$; (d) $\Gamma' = 1$.

dichroic polarizer [55], or a liquid-crystal converter [56]. The beam is sent to the sample (S). The emerging beam passes through a linear polarizer (P_2) with its transmission axis aligned with the x-axis. The transverse intensity profile of the beam can be observed on a screen (Σ) placed at an (arbitrary) distance from the sample, or recorded by a CCD camera.

This scheme reproduces the one presented to detect circular birefringence. The quantitative determination of Γ can be performed, for example, by measuring the irradiance at three points of the output beam cross section, located along a circle, centered on the origin of the axes and with an arbitrary radius, at the angles $\vartheta = \pi/4$, $\vartheta = 0$ $\vartheta = -\pi/4$, respectively. The irradiance values at these points are, from Eq. (48),

$$\begin{cases} I_0 = S_0^{out}(r, 0) = \alpha \left[\cosh(2\,\Gamma') + \cos(2\Gamma)\right] , \\ I_+ = S_0^{out}(r, \pi/4) = \alpha \left[\cosh(2\,\Gamma') - \sin(2\Gamma)\right] , \\ I_- = S_0^{out}(r, -\pi/4) = \alpha \left[\cosh(2\,\Gamma') + \sin(2\Gamma)\right] , \end{cases} \tag{49}$$

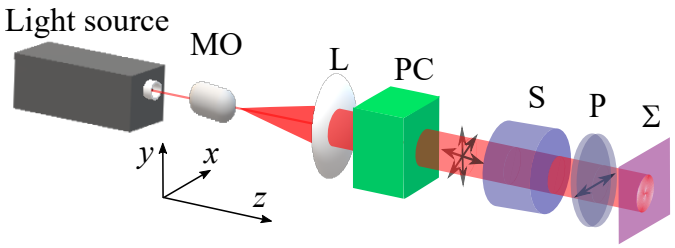

Figure 6: Proposed setup to detect circular birefringence and dichroism of chiral media. MO: microscope objective; L: lens; PC: polarization converter; P: linear polarizer; S: sample; Σ: screen.

with $\alpha = C\, S_0^{in}(r)$.

Solving Eq. (49) for $\cos(2\Gamma)$ and $\sin(2\Gamma)$ we have

$$\begin{cases} \cos(2\Gamma) = \dfrac{1}{\alpha}\left(I_0 - \dfrac{I_- + I_+}{2}\right), \\ \\ \sin(2\Gamma) = \dfrac{1}{\alpha}\left(\dfrac{I_- - I_+}{2}\right), \end{cases} \tag{50}$$

which allow for the unambiguous determination of Γ (except for the unavoidable periodicity of π) without measuring α.

Recovering Γ' from Eq. (49) would be also possible, because

$$\cosh(2\Gamma') = \frac{I_- + I_+}{2\alpha}, \tag{51}$$

but the knowledge of α is required and, moreover, only the absolute value of Γ' would be determined.

A more effective approach consists of slightly modifying the optical scheme of Fig. 6, inserting a quarter-wave plate in front of the sample whose neutral lines are aligned with the XY-axes, in such a way that the radially polarized input beam is converted into a beam of the form in Eq. (39). The presence of the linear polarizer after the sample changes the expression of the output beam irradiance, with respect to that obtained in Eq. (42) of Sec. 5, which in this case turns out to be

$$S_0^{out}(\boldsymbol{r}) = C\, S_0^{in}(\boldsymbol{r})\,[\cosh(2\,\Gamma') + \cos(2\vartheta)\,\cos(2\,\Gamma) - \sin(2\vartheta)\,\sinh(2\,\Gamma')]\,. \tag{52}$$

Therefore, the irradiance values at two points across the output plane, located along a circle centered on the axes origin and with arbitrary radius, at the angles $\vartheta = \pi/4$ and $\vartheta = -\pi/4$ are

$$\begin{cases} I'_+ = S_0^{out}(r, \pi/4) = \alpha \left[\cosh(2\,\Gamma') - \sinh(2\Gamma')\right] , \\ I'_- = S_0^{out}(r, -\pi/4) = \alpha \left[\cosh(2\,\Gamma') + \sinh(2\Gamma')\right] , \end{cases} \tag{53}$$

whence

$$\tanh(2\Gamma') \; = \frac{I'_- - I'_+}{I'_- + I'_+}, \tag{54}$$

from which Γ' can be recovered unambiguously.

7. Conclusions

The propagation of non-uniformly and totally polarized (NUTP) beams inside chiral media has been studied. A paraxial vector beam has been modeled as the superposition of Gaussian modes. For suitable choices of the component modes, the resulting beams present transverse polarization patterns that remain unchanged during propagation in free space or through ABCD optical systems. This property offers a significant advantage in many applications, because it allows the same transverse polarization pattern to be detected across any transverse plane. However, the property of being propagation-invariant is lost when beams of this kind pass through a chiral sample.

In this paper it has been shown that, if the beam impinging on the sample is suitably collimated, the Mueller formalisms can be used to derive the polarization of beam emerging from the sample, and the latter remains polarization-invariant during the subsequent free-space propagation.

The effects of chirality on the propagation of a NUTP incident beam have been studied under the above conditions. A significant result is that, by suitably choosing the input beam, a simple visual analysis of the transverse irradiance pattern of the output beam can give useful information about the circular dichroism and birefringence properties of the sample. Quantitative determinations of the optical parameters of the medium can be derived by measuring the irradiance at two or three distinct points (depending on the parameter to be measured) across any transverse plane of the output beam. A simple optical scheme has been presented to recover such parameters.

Acknowledgements

This work has been supported by Spanish Ministerio de Economía y Competitividad under project PID2023-148021NB-I00 and Project FASLIGTH (RED2022-134391-T).

Appendix

Here we derive the Jones matrix ($\widehat{J}$) and the Mueller matrix ($\widehat{M}$) of a chiral medium of thickness d.

To this aim, it is convenient to start from Jones vectors written in terms of circular right- and left-polarizations, instead of the usual ones, which use linear polarization states. With such a choice it is immediate to recognize that the Jones matrix of the element is expressed as

$$\begin{aligned} \widehat{J}_c &= \begin{pmatrix} e^{-ikd\tilde{n}_R} & 0 \\ 0 & e^{-ikd\tilde{n}_L} \end{pmatrix} = \\ &= \begin{pmatrix} e^{-ikdn_R} e^{-kd\kappa_R} & 0 \\ 0 & e^{-ikdn_L}\, e^{-kd\kappa_L} \end{pmatrix} , \end{aligned} \tag{55}$$

which is separable into the product of two commuting matrices:

$$\widehat{J}_c = \begin{pmatrix} e^{-ikdn_R} & 0 \\ 0 & e^{-ikdn_L} \end{pmatrix} \begin{pmatrix} e^{-kd\kappa_R} & 0 \\ 0 & e^{-kd\kappa_L} \end{pmatrix} . \tag{56}$$

The first one, which contains the real part of the refractive index, gives account of circular birefringence, while the other, with the imaginary part, represents circular dichroism,

To covert the above matrix into the corresponding one, to be used with usual Jones vectors, we have to introduce the unitary matrix $\widehat{P}_{c\to l}$, defined as [53]

$$\widehat{P}_{c\to l} = \frac{1}{\sqrt{2}} \begin{pmatrix} 1 & 1 \\ i & -i \end{pmatrix} . \tag{57}$$

which allows one to pass from circular to linear representations. Therefore

$$\widehat{J} = \widehat{P}_{c\to l}\, \widehat{J}_c\, \widehat{P}^{-1}_{c\to l}. \tag{58}$$

Applying this transformation rule to the Jones matrix given by Eq. (56) the following Jones matrix is obtained in terms of linear polarization states:

$$\begin{aligned}\widehat{J} &= e^{-i\frac{kd}{2}(n_D+n_L)}e^{-\frac{kd}{2}(\kappa_D+\kappa_L)} \\ &\times \begin{pmatrix} \cos(\Gamma - i\Gamma') & -\sin(\Gamma - i\Gamma') \\ \sin(\Gamma - i\Gamma') & \cos(\Gamma - i\Gamma') \end{pmatrix},\end{aligned} \tag{59}$$

where the quantities Γ and Γ' were defined in Eqs. (12) and (13).

The Mueller matrix corresponding to a sample characterized by the Jones matrix $\widehat{J}$ can be obtained as [53],

$$\widehat{M} = \widehat{\mathcal{L}}\left(\widehat{J}\otimes\widehat{J}^*\right)\widehat{\mathcal{L}}^{-1}, \tag{60}$$

where the matrix $\widehat{\mathcal{L}}$ is defined as

$$\widehat{\mathcal{L}} = \begin{pmatrix} 1 & 0 & 0 & 1 \\ 1 & 0 & 0 & -1 \\ 0 & 1 & 1 & 0 \\ 0 & \mathrm{i} & -\mathrm{i} & 0 \end{pmatrix}, \tag{61}$$

and $\otimes$ denotes the Kronecker product. Applying this relation to an optically active medium described by the Jones matrix in Eq. (59) we obtain (see, for example, [49, 51, 52, 57])

$$\widehat{M}_{AO} = e^{-kd(\kappa_R+\kappa_L)}\begin{pmatrix} \cosh 2\Gamma' & 0 & 0 & -\sinh 2\Gamma' \\ 0 & \cos 2\Gamma & -\sin 2\Gamma & 0 \\ 0 & \sin 2\Gamma & \cos 2\Gamma & 0 \\ -\sinh 2\Gamma' & 0 & 0 & \cosh 2\Gamma' \end{pmatrix}. \tag{62}$$

where cosh and sinh are the hyperbolic cosine and sine, respectively.

References

[1] Y. Mushiake, K. Matsumura, N. Nakajima, Generation of radially polarized optical beam mode by laser oscillation, Proceedings of the IEEE 60 (9) (1972) 1107–1109. doi:10.1109/PROC.1972.8865.

[2] S. C. Tidwell, D. H. Ford, W. D. Kimura, Generating radially polarized beams interferometrically, Appl. Opt. 29 (15) (1990) 2234–2239. doi:10.1364/AO.29.002234.
URL http://ao.osa.org/abstract.cfm?URI=ao-29-15-2234

[3] T. Erdogan, O. King, G. W. Wicks, D. G. Hall, E. H. Anderson, M. J. Rooks, Concentric-circle-grating, surface-emitting semiconductor lasers, Opt. Photon. News 3 (12) (1992) 41–41. doi:10.1364/OPN.3.12.000041.
URL http://www.osa-opn.org/abstract.cfm?URI=opn-3-12-41

[4] X.-L. Wang, J. Ding, W.-J. Ni, C.-S. Guo, H.-T. Wang, Generation of arbitrary vector beams with a spatial light modulator and a common path interferometric arrangement, Opt. Lett. 32 (24) (2007) 3549–3551. doi:10.1364/OL.32.003549.
URL https://opg.optica.org/ol/abstract.cfm?URI=ol-32-24-3549

[5] P. García-Martínez, D. Marco, J. L. Martínez-Fuentes, M. del Mar Sánchez-López, I. Moreno, Efficient on-axis SLM engineering of optical vector modes, Optics and Lasers in Engineering 125 (2020) 105859. doi:https://doi.org/10.1016/j.optlaseng.2019.105859.
URL https://www.sciencedirect.com/science/article/pii/S0143816619309959

[6] J. A. Davis, I. Moreno, M. del Mar Sánchez-López, D. M. Cottrell, Vector beams generated with a Fourier transform processor with geometric phase grating, Optical Engineering 62 (1) (2023) 013104. doi:10.1117/1.OE.62.1.013104.
URL https://doi.org/10.1117/1.OE.62.1.013104

[7] E. J. Galvez, S. Khadka, W. H. Schubert, S. Nomoto, Poincaré-beam patterns produced by nonseparable superpositions of Laguerre-Gauss and polarization modes of light, Appl. Opt. 51 (15) (2012) 2925–2934. doi:10.1364/AO.51.002925.
URL http://ao.osa.org/abstract.cfm?URI=ao-51-15-2925

[8] F. Gori, Polarization basis for vortex beams, J. Opt. Soc. Am. A 18 (7) (2001) 1612–1617. doi:10.1364/JOSAA.18.001612.
URL http://josaa.osa.org/abstract.cfm?URI=josaa-18-7-1612

[9] H. Guo, J. Chen, S. Zhuang, Vector plane wave spectrum of an arbitrary polarized electromagnetic wave, Opt. Express 14 (6) (2006) 2095–2100. doi:10.1364/OE.14.002095.

URL https://opg.optica.org/oe/abstract.cfm?URI=oe-14-6-2095

[10] G. Zhou, Analytical vectorial structure of laguerre-gaussian beam in the far field, Opt. Lett. 31 (17) (2006) 2616–2618. doi:10.1364/OL.31.002616.
URL https://opg.optica.org/ol/abstract.cfm?URI=ol-31-17-2616

[11] D. Deng, Q. Guo, Analytical vectorial structure of radially polarized light beams, Opt. Lett. 32 (18) (2007) 2711–2713. doi:10.1364/OL.32.002711.
URL https://opg.optica.org/ol/abstract.cfm?URI=ol-32-18-2711

[12] G. Milione, S. Evans, D. A. Nolan, R. R. Alfano, Higher order Pancharatnam-Berry phase and the angular momentum of light, Phys. Rev. Lett. 108 (2012) 190401. doi:10.1103/PhysRevLett.108.190401.
URL https://link.aps.org/doi/10.1103/PhysRevLett.108.190401

[13] S. Chen, X. Zhou, Y. Liu, X. Ling, H. Luo, S. Wen, Generation of arbitrary cylindrical vector beams on the higher order Poincaré sphere, Opt. Lett. 39 (18) (2014) 5274–5276. doi:10.1364/OL.39.005274.
URL http://ol.osa.org/abstract.cfm?URI=ol-39-18-5274

[14] Q. Zhan, Cylindrical vector beams: from mathematical concepts to applications, Adv. Opt. Photon. 1 (1) (2009) 1–57. doi:10.1364/AOP.1.000001.
URL http://aop.osa.org/abstract.cfm?URI=aop-1-1-1

[15] X. Zhu, J. Yu, F. Wang, Y. Chen, Y. Cai, O. Korotkova, Synthesis of vector nonuniformly correlated light beams by a single digital mirror device, Opt. Lett. 46 (12) (2021) 2996–2999. doi:10.1364/OL.428508.
URL http://www.osapublishing.org/ol/abstract.cfm?URI=ol-46-12-2996

[16] H. Rubinsztein-Dunlop, A. Forbes, M. V. Berry, M. R. Dennis, D. L. Andrews, M. Mansuripur, C. Denz, C. Alpmann, P. Banzer, T. Bauer,

E. Karimi, L. Marrucci, M. Padgett, M. Ritsch-Marte, N. M. Litchinitser, N. P. Bigelow, C. Rosales-Guzmán, A. Belmonte, J. P. Torres, T. W. Neely, M. Baker, R. Gordon, A. B. Stilgoe, J. Romero, A. G. White, R. Fickler, A. E. Willner, G. Xie, B. McMorran, A. M. Weiner, Roadmap on structured light, Journal of Optics 19 (1) (2017) 013001. URL http://stacks.iop.org/2040-8986/19/i=1/a=013001

[17] C. H. Krishna, S. Roy, Generation of inhomogeneously polarized vector vortex modes in few mode optical fiber, Optical and Quantum Electronics 51 (2) (2019) 41. doi:10.1007/s11082-019-1752-9.
URL https://doi.org/10.1007/s11082-019-1752-9

[18] J. Zhang, J. Xie, D. Deng, Second-order statistics of a partially coherent electromagnetic rotating elliptical gaussian vortex beam through non-kolmogorov turbulence, Opt. Express 26 (16) (2018) 21249–21257. doi:10.1364/OE.26.021249.
URL https://opg.optica.org/oe/abstract.cfm?URI=oe-26-16-21249

[19] C. Sun, X. Lv, B. Ma, J. Zhang, D. Deng, W. Hong, Statistical properties of partially coherent radially and azimuthally polarized rotating elliptical gaussian beams in oceanic turbulence with anisotropy, Opt. Express 27 (8) (2019) A245–A256. doi:10.1364/OE.27.00A245.
URL https://opg.optica.org/oe/abstract.cfm?URI=oe-27-8-A245

[20] G. Piquero, R. Martínez-Herrero, J. C. G. de Sande, M. Santarsiero, Synthesis and characterization of non-uniformly totally polarized light beams: tutorial, J. Opt. Soc. Am. A 37 (4) (ts) 591–605. doi:10.1364/JOSAA.379439.
URL http://josaa.osa.org/abstract.cfm?URI=josaa-37-4-591

[21] J. C. G. de Sande, M. Santarsiero, G. Piquero, Spirally polarized beams for polarimetry measurements of deterministic and homogeneous samples, Optics and Lasers in Engineering 91 (2017) 97 – 105. doi:http://dx.doi.org/10.1016/j.optlaseng.2016.11.008.
URL http://www.sciencedirect.com/science/article/pii/S0143816616304171

[22] J. C. Suárez-Bermejo, J. C. G. de Sande, M. Santarsiero, G. Piquero, Mueller matrix polarimetry using full Poincaré beams, Optics and Lasers in Engineering 122 (2019) 134 – 141. doi:https://doi.org/10.1016/j.optlaseng.2019.05.030.
URL http://www.sciencedirect.com/science/article/pii/S0143816619302805

[23] J. C. Suárez-Bermejo, J. Gorgas, S. Pascual, M. Santarsiero, J. C. G. de Sande, G. Piquero, Bayesian inference approach for full Poincaré Mueller polarimetry, Optics & Laser Technology 168 (2024) 109983. doi:https://doi.org/10.1016/j.optlastec.2023.109983.
URL https://www.sciencedirect.com/science/article/pii/S0030399223008769

[24] A. McWilliam, M. A. A. Khafaji, S. J. Svensson, S. ao Pádua, S. Franke-Arnold, Dynamic mueller matrix polarimetry using generalized measurements, Opt. Express 32 (12) (2024) 21909–21924. doi:10.1364/OE.521069.
URL https://opg.optica.org/oe/abstract.cfm?URI=oe-32-12-21909

[25] X.-B. Hu, C.-X. Liu, Y.-C. Zhu, R.-P. Chen, B. Zhao, F.-M. Wu, C. Rosales-Guzmán, Inhomogeneous enantiomeric solution concentration measurement harnessing vectorial structured light, ACS Photonics 11 (11) (2024) 4533–4540. arXiv:https://doi.org/10.1021/acsphotonics.4c00652, doi:10.1021/acsphotonics.4c00652.
URL https://doi.org/10.1021/acsphotonics.4c00652

[26] D. H. Goldstein, Polarized Light, second (revised and expanded) Edition, Marcel Dekker, Inc., 2003.

[27] R. Ribeiro, A. Fiasca, P. dos Santos, Automatic optical activity measurement system, Optics & Laser Technology 30 (2) (1998) 121–124. doi:https://doi.org/10.1016/S0030-3992(98)00025-5.
URL https://www.sciencedirect.com/science/article/pii/S0030399298000255

[28] K. E. van Holde, Physical Biochemistry, Prentice Hall, Enlgewood Cliffs, New Jersey., 1985.

[29] C. R. Cantor, P. R. Schimmel, Biophysical Chemistry. Part II: Techniques for the study of biological structure and function, W. H. Freeman and Company. New York., 1980.

[30] P. Gupta, A. Islam, F. Ahmad, M. I. Hassan, Applications of Circular Dichroism Spectroscopy in Studying Protein Folding, Stability, and Interaction, Springer Nature Singapore, Singapore, 2023, pp. 1–23. doi:10.1007/978-981-99-2079-2_1.
URL https://doi.org/10.1007/978-981-99-2079-2_1

[31] D. W. Green, J.-M. Lee, E.-J. Kim, D.-J. Lee, H.-S. Jung, Chiral biomaterials: From molecular design to regenerative medicine, Advanced Materials Interfaces 3 (6) (2016) 1500411. arXiv:https://onlinelibrary.wiley.com/doi/pdf/10.1002/admi.201500411, doi:https://doi.org/10.1002/admi.201500411.
URL https://onlinelibrary.wiley.com/doi/abs/10.1002/admi.201500411

[32] R. L. S. Lima, E. S. d. Silva, P. T. Araujo, N. M. B. Neto, Stokes spectropolarimetry applied to measure circular birefringence dispersion of aqueous solutions of sugars, Chirality 37 (7) (2025) e70047, e70047 CHIR-25-0030. arXiv:https://onlinelibrary.wiley.com/doi/pdf/10.1002/chir.70047, doi:https://doi.org/10.1002/chir.70047.
URL https://onlinelibrary.wiley.com/doi/abs/10.1002/chir.70047

[33] D. M. Gray, Circular Dichroism of Protein-Nucleic Acid Interactions, Springer US, Boston, MA, 1996, pp. 469–500. doi:10.1007/978-1-4757-2508-7_13.
URL https://doi.org/10.1007/978-1-4757-2508-7_13

[34] F. Zhu, N. W. Isaacs, L. Hecht, L. D. Barron, Raman optical activity: A tool for protein structure analysis, Structure 13 (10) (2005) 1409–1419. doi:https://doi.org/10.1016/j.str.2005.07.009.
URL https://www.sciencedirect.com/science/article/pii/S0969212605002686

[35] F. Zhuang, X. Du, D. Zhao, Polarization modulation for a stochastic electromagnetic beam passing through a chiral medium, Opt. Lett.

36 (14) (2011) 2683–2685. doi:10.1364/OL.36.002683.
URL https://opg.optica.org/ol/abstract.cfm?URI=ol-36-14-2683

[36] F. Zhuang, X. Du, Y. Ye, D. Zhao, Evolution of airy beams in a chiral medium, Opt. Lett. 37 (11) (2012) 1871–1873. doi:10.1364/OL.37.001871.
URL https://opg.optica.org/ol/abstract.cfm?URI=ol-37-11-1871

[37] S. Hua, Y. Liu, H. Zhang, L. Tang, Y. Feng, Propagation of an airy-gaussian-vortex beam in a chiral medium, Optics Communications 388 (2017) 29–37. doi:https://doi.org/10.1016/j.optcom.2016.11.001.
URL https://www.sciencedirect.com/science/article/pii/S003040181630966X

[38] K. Zhou, J. Zhang, H. Mo, J. Chen, X. Yang, Z. Lai, X. Chen, X. Yang, D. Deng, Propagation of the chirped-airy–gaussian-vortex beams in the chiral medium, Journal of Optics 20 (7) (2018) 075601. doi:10.1088/2040-8986/aac4c6.
URL https://dx.doi.org/10.1088/2040-8986/aac4c6

[39] J. Xie, J. Zhang, J. Ye, H. Liu, Z. Liang, S. Long, K. Zhou, D. Deng, Paraxial propagation of the first-order chirped airy vortex beams in a chiral medium, Opt. Express 26 (5) (2018) 5845–5856. doi:10.1364/OE.26.005845.
URL https://opg.optica.org/oe/abstract.cfm?URI=oe-26-5-5845

[40] H. Xu, S. Wu, Y. Wu, X. Hu, K.-H. Chew, R.-P. Chen, Vectorial acousto-optic raman–nath diffraction effect of chiral liquid media, Opt. Lett. 50 (3) (2025) 936–939. doi:10.1364/OL.545201.
URL https://opg.optica.org/ol/abstract.cfm?URI=ol-50-3-936

[41] B. Kumar Das, C. Granados Buitrago, M. F. Ciappina, Propagation of perfect optical vortex beams in a chiral medium, Journal of Optics 27 (7) (2025) 075603. doi:10.1088/2040-8986/ade815.
URL https://dx.doi.org/10.1088/2040-8986/ade815

[42] E. Abramochkin, V. Volostnikov, Beam transformations and non-transformed beams, Optics Communications 83 (1) (1991) 123 – 135. doi:https://doi.org/10.1016/0030-4018(91)90534-K.
URL http://www.sciencedirect.com/science/article/pii/003040189190534K

[43] A. E. Siegman, Lasers, University Science Books, 1986.

[44] E. Otte, C. Denz, Sculpting complex polarization singularity networks, Opt. Lett. 43 (23) (2018) 5821–5824. doi:10.1364/OL.43.005821.
URL http://ol.osa.org/abstract.cfm?URI=ol-43-23-5821

[45] J. C. G. de Sande, G. Piquero, J. C. Suárez-Bermejo, M. Santarsiero, Beams with propagation-invariant transverse polarization pattern (2021). arXiv:2102.00024.

[46] J. C. G. de Sande, G. Piquero, J. C. Suárez-Bermejo, M. Santarsiero, Mueller matrix polarimetry with invariant polarization pattern beams, Photonics 8 (11) (2021). doi:10.3390/photonics8110491.
URL https://www.mdpi.com/2304-6732/8/11/491

[47] R. Chipman, W. Lam, G. Young, Polarized Light and Optical Systems, Optical Sciences and Applications of Light, CRC Press, 2018.
URL https://books.google.es/books?id=KwFlDwAAQBAJ

[48] M. Born, E. Wolf, Principles of Optics: Electromagnetic Theory of Propagation, Interference and Diffraction of Light (7th Edition), 7th Edition, Cambridge University Press, 1999.

[49] B. Bakhouche, H. Moussaoui, H. Bendada, Combined Jones and Mueller matrix method for the evaluation the optical rotation and circular dichroism in chiral medium, Optik 271 (2022) 170219. doi:https://doi.org/10.1016/j.ijleo.2022.170219.
URL https://www.sciencedirect.com/science/article/pii/S0030402622014772

[50] P. Cortés, G. Piquero, J. C. G de Sande, Chiral media and optical rotatory dispersion by means of a simple polarimetric experiment for undergraduate students, European Journal of Physics 45 (5) (2024) 055303. doi:10.1088/1361-6404/ad695d.
URL https://dx.doi.org/10.1088/1361-6404/ad695d

[51] H. Arwin, S. Schoeche, J. Hilfiker, M. Hartveit, K. Järrendahl, O. R. Juárez-Rivera, A. Mendoza-Galván, R. Magnusson, Optical chirality determined from Mueller matrices, Applied Sciences 11 (15) (2021). doi:10.3390/app11156742.
URL https://www.mdpi.com/2076-3417/11/15/6742

[52] D. Vala, M. Mičica, K. Postava, Molecular chirality from the viewpoint of Mueller ellipsometry, in: J. Masajada, W. Urbańczyk (Eds.), 22nd Polish-Slovak-Czech Optical Conference on Wave and Quantum Aspects of Contemporary Optics, Vol. 12502, International Society for Optics and Photonics, SPIE, 2022, p. 1250210. doi:10.1117/12.2664191.
URL https://doi.org/10.1117/12.2664191

[53] J. J. Gil, R. Ossikovski, Polarized Light and the Mueller Matrix Approach, CRC Press Taylor & Francis Group, Boca Raton, 2016. doi:10.1201/b19711.

[54] J. Qi, W. Wang, B. Shi, H. Zhang, Y. Shen, H. Deng, W. Pu, X. Liu, H. Shan, X. Ma, L. Zhang, W. Lu, M. Fu, X. Li, Concise and efficient direct-view generation of arbitrary cylindrical vector beams by a vortex half-wave plate, Photon. Res. 9 (5) (2021) 803–813. doi:10.1364/PRJ.419561.
URL https://opg.optica.org/prj/abstract.cfm?URI=prj-9-5-803

[55] W. Zhang, Z. Zhang, Scanning visible polarization-direction-modulation polarimeter for optically active media measurement, Sensors and Actuators B: Chemical 286 (2019) 119–124. doi:https://doi.org/10.1016/j.snb.2019.01.139.
URL https://www.sciencedirect.com/science/article/pii/S0925400519301674

[56] M. Stalder, M. Schadt, Linearly polarized light with axial symmetry generated by liquid-crystal polarization converters, Opt. Lett. 21 (23) (1996) 1948–1950. doi:10.1364/OL.21.001948.
URL https://opg.optica.org/ol/abstract.cfm?URI=ol-21-23-1948

[57] P. Sun, Y. Ma, W. Liu, Q. Yang, Q. Jia, Mueller matrix decomposition for determination of optical rotation of glucose molecules in

turbid media, Journal of Biomedical Optics 19 (4) (2014) 046015. doi:10.1117/1.JBO.19.4.046015.
URL https://doi.org/10.1117/1.JBO.19.4.046015